Acta Physiologica Sinica, October 25, 2011, 63(5): 401−411
http://www.actaps.com.cn

Invited Review

Computational modeling of the dynamics of simple and complex cells in primary visual cortex

TAO Louis[1,*], CAI David[2,3]

[1]Center for Bioinformatics, National Laboratory of Protein Engineering and Plant Genetics Engineering, College of Life Sciences, Peking University, Beijing 100871, China; [2]Institute of Natural Sciences & Department of Mathematics, Shanghai Jiao Tong University, Shanghai 200240, China; [3]Courant Institute of Mathematical Sciences and Center for Neural Science, New York University, New York, NY 10012, USA

Abstract: We review our work on computational modeling of the mammalian visual cortex. In particular, we explain the network mechanism of how simple and complex cells arise in a large scale neuronal network model of primary visual cortex. The simple cells are so-called because they respond approximately linearly to visual stimulus, whereas the complex cells exhibit nonlinear response to visual stimulation. Our model reproduces qualitatively the experimentally observed distributions of simple and complex cells.

Key words: primary visual cortex; mathematical modeling; neuronal networks; spatial summation; orientation selectivity; nonlinear dynamics

初级视觉皮层“简单”与“复杂”神经元动力学的计算建模

陶乐天[1,*], 蔡申瓯[2,3]

[1]北京大学生命科学学院生物信息中心，蛋白质工程及植物基因工程国家重点实验室，北京 100871；[2]上海交通大学自然科学研究院和数学系，上海 200240；[3]美国纽约大学库朗数学研究所和神经科学中心，纽约 NY 10012

摘 要：本文回顾了我们在哺乳动物视觉皮层的建模工作。利用初级视觉皮层的大规模神经元网络模型，我们解释了初级视觉皮层里“简单”与“复杂”神经元现象的网络机制。所谓的“简单”细胞对视觉刺激的反应近似线性，而“复杂”细胞对视觉刺激是非线性的。我们的模型成功地再现了简单和复杂细胞分布的实验数据。

关键词：初级视皮层；数学模型；神经元网络；视觉信号空间总和；朝向选择性；非线性动力学
中图分类号：O242.1；O29；Q189

Located in the back of the neocortex, the mammalian primary visual cortex (V1) is a thin sheet of densely packed and highly interconnected neurons. Along the “visual pathway” (retina-thalamus-V1-V2 and beyond), it is in V1 that neuronal responses are first simultaneously selective to many elementary features of visual scenes, including a pattern’s orientation. For instance, the orientation tuning property of a neuron is its active response to some orientations of a simple visual pattern, say, a bar or a grating, but not to other orientations [1].

Anatomically, V1 is several cm squared in lateral area and 1–2 mm in thickness. It has a laminar structure, in which each layer is anatomically distinct and contains both excitatory and inhibitory neurons. Within each layer, the lateral connectivity is locally dense, along with highly specific feed-forward and feed-back

This work was partially supported by National Science Foundation of USA (No. DMS-1009575), and the National Basic Research Development Program of China (973 Program, No. 2011CB809105).

*Corresponding author. Tel: +86-10-62755206; E-mail: taolt@cbi.pku.edu.cn

projections between the different layers. Visual stimulus from the outside world first arrives in V1 via axonal projections from the neurons in the lateral geniculate nucleus (LGN) in the thalamus. These thalamocortical inputs are excitatory only and project primarily into the layers 4Cα ("magno pathway"), 4Cβ ("parvo pathway") and 6.

Physiologically, neurons in V1 can be roughly divided into "simple" and "complex" cells. This classical division dates back to the 1960s [1]. The neurons whose responses to visual stimuli are approximately linear are termed "simple," whereas those remaining neurons with nonlinear responses are called "complex." For instance, if the stimulus is a drifting grating, the firing rate of a prototypical simple cell is modulated at the frequency at which the grating drifts through the neuron's receptive field. In contrast, the firing rate of a complex cell will change with the onset of the stimulus, but then stay basically constant in time during the entire stimulus presentation. For a stationary, contrast-reversing, sinusoidally modulated grating, simple-cell firing rates are sensitive to the location of the grating (i.e. the spatial phase of the sinusoidal grating) and are modulated at the stimulus frequency, whereas complex cells are insensitive to the location of the grating, and have firing rates that are modulated at double the stimulus frequency (a classical sign for nonlinearity)[2, 3].

Simple and complex cells may have different tasks in visual perception. Cortical cells must represent spatial properties such as surface brightness and color, and the perceptual spatial organization of a scene that is the basis of form. Simple cells are assumed to be necessary for all of these functions because they are the V1 neurons that are able to respond monotonically to signed edge contrast. Complex cells, being insensitive to spatial phase, cannot provide a cortical representation of signed contrast, but they are sensitive to texture, firing at elevated rates in response to stimuli within their receptive fields.

The long-standing, theoretical model [1] hypothesizes that the simple cells receive inputs from the LGN and pool their output to drive the responses of complex cells. Thus the spatial phase sensitivity of simple cells can be lost if the spatial pooling driving complex cells is non-specific (i.e. independent of phase). This model is supported by the physiological evidence for excitatory connections from simple cells to complex ones [4].

While long-standing, the simple/complex classification is hardly sharp. Recent work by Ringach *et al*. [5] analyzes the extracellular responses of neurons in macaque V1 experiments. They find that many V1 cells are neither completely simple nor completely complex, but lie somewhere in between. And while most cells in V1 might be classified as complex, the cortical layer which receives the bulk of LGN excitation, 4Cα, has simple and complex cells in approximately equal proportion [5].

Furthermore, many experiments show that complex cells receive inputs not just from simple cells, but also receive strong input from other complex cells [4] and even directly from the LGN [6–8]. Many experiments show that some complex cells can be excited without strongly exciting simple cells [9–13].

Therefore, we consider an alternative hypothesis that the amount of excitatory LGN input varies from one V1 neuron to the next (indirect evidence for this is given previously [14–16]), and is compensated by the amount of cortical excitation, so that each V1 neuron receives roughly the same amount of excitation [17], as suggested by cortical development theories [18, 19] and experiments [20, 21].

1 Computational model

We adopt this hypothesis in our recent work. In a series of papers [17, 22–24], we have developed a computational model of a small, local patch of V1 layer 4Cα, which is the primary input layer in macaque V1. This cortical neuronal network model contains four orientation hypercolumns with pinwheel centers within a 1 mm^2 patch. For simplicity, the boundary conditions are taken to be periodic (Fig. 1).

Individual neurons are modeled as conductance-based, linear integrate-and-fire (I&F) point neurons [25] (i.e., all spatial effects within a single cell are neglected). Between "spike times" the intra-cellular potentials v^j evolve in time according to the following linear differential equation:

$$\frac{dv^j}{dt} = -g_L(v^j - V_R) - \left(g^j_{LGN}(t) + g^j_E(t)\right)\left(v^j - V_E\right) - \left(g^j_I(t) + f^j_{INH}(t)\right)\left(v^j - V_I\right)$$

Here V_R, V_E, V_I are the rest, excitatory, and inhibitory reversal potentials, respectively; g_L is the leak conductance. Neurons are coupled to each other via the cortico-cortical conductance terms, $g^j_E(t)$ and $g^j_I(t)$, which are dependent on individual neuronal spike times. Therefore, to specify these conductances, we need to

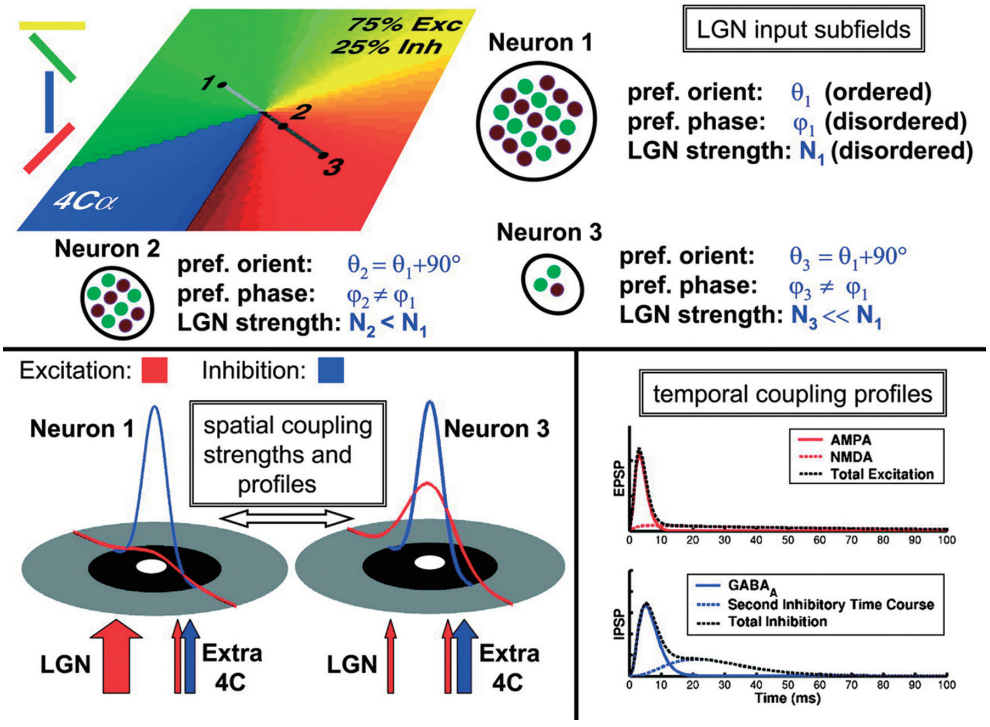

Fig. 1. Schematic of model. Upper panel: Inputs from the visual stimulus, as relayed through the LGN. Each primary visual cortex (V1) neuron receives (excitatory) visual stimulation through a collection of LGN cells that is probabilistically chosen from a two-dimensional Gabor function. Orientation preference is laid out in pinwheels (color map) and the spatial phase preference is distributed randomly (map not shown, but examples are shown for 3 neurons). Lower left: Intracortical couplings are isotropic and are modeled to be Gaussians in space (excitation in red and inhibition in blue). Lower right: Each cortico-cortical postsynaptic conductance is modeled as a single or a sum of alpha functions. The figure is reproduced from Tao *et al*. [17].

compute the m^{th} spike time of the j^{th} model neuron, t_m^j, which is determined by $v^j\left(t_{m-}^j\right)=V_T$, i.e., by the time at which the neuron's membrane potential reaches a threshold. Then the membrane potential is reset to the rest potential and held at rest for an absolute refractory period, τ_{ref}: $v^j\left(t_m^j+\tau_{ref}\right)=V_R$. We take $\tau_{ref}=3(1)$ ms for excitatory (inhibitory) neurons. The various synaptic potentials are ordered $V_I<V_R<V_T<V_E$, and therefore, the term $-g_E^j(t)\left(v^j-V_E\right)$ drives the voltage up and can be considered "excitatory", while $-g_I^j(t)\left(v^j-V_I\right)$ drives the voltage down and can be considered "inhibitory" .

To close the system of equations, we need to specify the time-dependent conductances, $g_{LGN}^j(t)$, $g_E^j(t)$ and $g_I^j(t)$, which are produced by spiking activity from the LGN and from within the model cortex. The time-dependent postsynaptic conductances (PSCs) also arise due to visual stimulation (as relayed via the retina and the LGN). Overall, the PSCs have the general form

$$g_{LGN}^j(t)=f_E\sum_l G_E(t-s_l^j)$$

$$f_{INH}^j(t)=f_I\sum_l G_I(t-s_l^j)$$

$$g_E^j(t)=S_E^j\sum_k K_{j,k}^E\sum_l G_E(t-t_l^k)$$

$$g_I^j(t)=S_I^j\sum_k K_{j,k}^I\sum_l G_I(t-t_l^k)$$

where f_E is the excitatory LGN input strength, f_I is the strength of the inhibitory noise; $S_{E,I}^j$ are the intra-cortical excitatory and inhibitory (resp.) coupling constants for neuron j; $G_{E,I}$ models the temporal forms of individual excitatory and inhibitory PSCs, and is taken to be alpha functions (i.e., difference of exponentials): $G_\sigma(t)=\theta(t)\left[\exp\left(-t/\tau_\sigma^d\right)-\exp\left(-t/\tau_\sigma^r\right)\right]/\left(\tau_\sigma^d-\tau_\sigma^r\right)$, $\sigma=$ *E, I*; we set $\tau_\sigma^r=1, 2, 1$ ms, $\tau_\sigma^d=3, 80, 10$ ms for AMPA, NMDA and $GABA_A$, respectively (shown as temporal coupling profiles in the lower right panel of Fig. 1).

The kernels $K_{j,k}^E$ and $K_{j,k}^I$ denote the element of the excitatory (inhibitory) connectivity coupling neurons j

and k and models the spatial structure of the cortical coupling; They are normalized to have unit sum so that the $S^j_{E,I}$'s denote synaptic strengths (lower left panel of Fig. 1).

The collective LGN drive into a single neuron, $g^j_{LGN}(t)$, is modeled as time-dependent Poisson spike trains whose rate is given by the sum of linear spatio-temporal filters. Response properties of individual LGN cells are estimated from experimental studies [26–28]. Individual LGN neuron has a classical "center-surround" (on-off) receptive field and thus shows no orientation selectivity. There are two types of such neurons: on-center and off-center. For an on-center neuron, illuminating the center of its receptive field increases its firing rate, while illuminating a surrounding annulus decreases it. For an off-center neuron, the respective responses are exactly the opposite. The temporal response curve of an LGN neuron increases to a maximum at about 40 ms, to a sub-background response with a minimum at about 60 ms, has zero over all integral (which holds for LGN cells in the magno pathway), and is taken from previous reports [29–31]. Since the LGN does not generate inhibitory PSC in V1 cells, inhibition arises from the LGN driving inhibitory neurons, and this is sometimes referred to as a "feed-forward" inhibition. The inhibitory noise conductance $f^j_{INH}(t)$ is modeled as a homogeneous Poisson spike train.

In our models, an individual V1 neuron "sees" the world through the pooling of about $N_{LGN} \sim 20$ LGN cells [16] (See Fig. 1 for examples and the overall schematic). Thus the LGN input into a single V1 neuron is represented by a sum of Poisson spike trains, with total rate given by

$$\nu^j_{LGN}(t) = \sum_{k=1}^{N^j_{LGN}} \left\{ R_0 \pm \int_{\mathbb{R}^2} d\vec{x} K_{LGN}\left(\left|\vec{x}-\vec{x}_k\right|\right) \int_{-\infty}^{t} ds G_{LGN}(t-s) I(\vec{x},s) \right\}^+$$

Here R_0 is the background LGN firing rate (about 10–20 Hz). The ±-sign models the processing of on-center and off-center neurons. The superscripted plus sign signifies rate rectification. The exact forms of the LGN kernels K_{LGN} and G_{LGN} are given in Tao *et al*. and Wielaard *et al.* [17, 22]. In particular, to model the "center-surround" receptive fields of the LGN neurons, K_{LGN} is taken to be a difference of two Gaussian functions, with parameters as in Somers *et al*. and Troyer *et al.* [32, 33]. The kernel G_{LGN} is taken directly from previous reports [29–31].

The summed LGN input conductance driving individual V1 neurons is highly structured: The on- and off-centered LGN cells at $\vec{x}_k$ are segregated into elongated sub-regions and are arrayed in a Gabor-like pattern [14, 34], tilted by a preferred angle θ and a spatial phase ϕ. In the network model, the spatial variation of this summed LGN input is responsible for the organization of both orientation preference and spatial phase preference. Orientation preferences are laid out in pinwheel patterns, and the preferred spatial phase varies randomly from neuron to neuron (consistent with recent experimental findings [35, 36]).

A central assumption of this model is that the strength of LGN excitation varies broadly, so that some cortical cells receive significant LGN drive, while others receive little. This is combined with the constraint that the total excitatory synaptic drive onto each cell is approximately constant, though divided between geniculate and cortical sources, as is suggested by theories of cortical development [18, 19] and by recent experiments [20, 21]. Thus to capture the diversity of feed-forward input as seen in experiments, we assume that N^j_{LGN}, the number of LGN cells with outputs converging on the j^{th} V1 neuron, is distributed randomly and uniformly between 0 and 30, and is also distributed randomly in space. As a result, some cortical cells receive significant LGN drive while their neighbors may receive little LGN excitation. Finally, this is combined with the constraint that the total excitatory synaptic drive onto each cell is approximately constant, though divided between LGN and cortico-cortical, therefore those neurons receiving weak or no LGN drive, receive stronger recurrent excitation S^j_E.

As the results below show, these basic model assumptions naturally lead to neuronal population response diversity consistent with recent experiments. The aim of our modeling is to understand the function of the V1 cortical network in terms of its network structure and dynamics. Thus to be successful, the model must account in a realistic manner for orientation selectivity, response dynamics with a wide range of input stimuli, firing rate patterns in background, as well as during stimulation. In this review, we focus on the model's performance in spatial summation experiments that have been used to classify neurons as simple or complex. We show that this egalitarian model, which combines natural assumptions on the variability of cortical and geniculate drive and what is known about the neuronal architecture of V1, can rationalize many aspects of the available experimental data. The model

yields physiologically realistic simple and complex cell responses, both in the mean firing rates and their temporal form. The architecture leads to distinctive predictions of population measures of simple/complex responses, which have the qualitative structure seen in recent experimental measurements .

2 Modeling results

In this review, we will focus on the following two types of visual stimuli:

Contrast reversal: $I(\vec{x},t)=I_0\left[1+\varepsilon\sin\left(\vec{k}\cdot\vec{x}+\phi\right)\sin(\omega t)\right]$

Drifting grating: $I(\vec{x},t)=I_0\left[1+\varepsilon\sin\left(\vec{k}\cdot\vec{x}-\omega t+\phi\right)\right]$

I_0 is the average intensity, $\varepsilon<1$ is the stimulus contrast, the wave vector $\vec{k}=k(\cos\theta,\sin\theta)$ is parameterized by spatial frequency k and orientation θ; ω is the temporal frequency and ϕ is the spatial phase.

2.1 Contrast reversal and spatial phase dependence

"Contrast reversal" is the sinusoidal modulation in time of the contrast of a standing sine-wave pattern. Response to contrast reversal is a critical test of linearity in simple cells [37, 38]. A simple cell's response depends strongly upon the spatial phase ϕ (i.e. the position) of the standing grating pattern relative to the midpoint of the neuron's receptive field, has a large amplitude response at the fundamental driving frequency at one spatial phase (the "preferred-phase"), and very little response at the "orthogonal phase", 90° away from the preferred. Responses at both of these phases show little or no generation of the higher temporal harmonics that might be expected for a nonlinear system. On the other hand, nonlinear harmonic distortion products are apparent in the responses of cortical complex cells [37]: Their temporal responses show little sensitivity to spatial phase, and firing modulates at twice the stimulus frequency (i.e., at the second harmonic).

Simple and complex cell responses, like those seen in experiment, arise in this model cortex. For contrast reversal, Fig. 2*A* shows a model cell responding like a simple cell, and Fig. 2*B* shows another cell responding like a complex cell. These are but two cells taken from a large-scale network simulation with about 4 000 cells (of which 75% are excitatory, and 25% are inhibitory).

Let us consider how a complex cell might arise in a network. Imagine a network neuron receiving little or no LGN input and instead has its response driven by cortico-cortical inputs. In a network of simple cells and complex cells, a contrast-reversing grating over one cycle of stimulation would necessarily drive neurons with different spatial phase preferences, and a non-specific pooling of the outputs of these neurons would produce synaptic inputs that are frequency doubled. In Fig. 3, we display such a cell driven by contrast-reversing gratings at two different spatial phases. The sample neuron samples through its synaptic inputs the activity of many other cells in the network, each responding at a different input phase. Consequently, the synaptic inputs reflect the bulk forcing and are therefore frequency doubled. Since the spatial pooling is non-specific and is

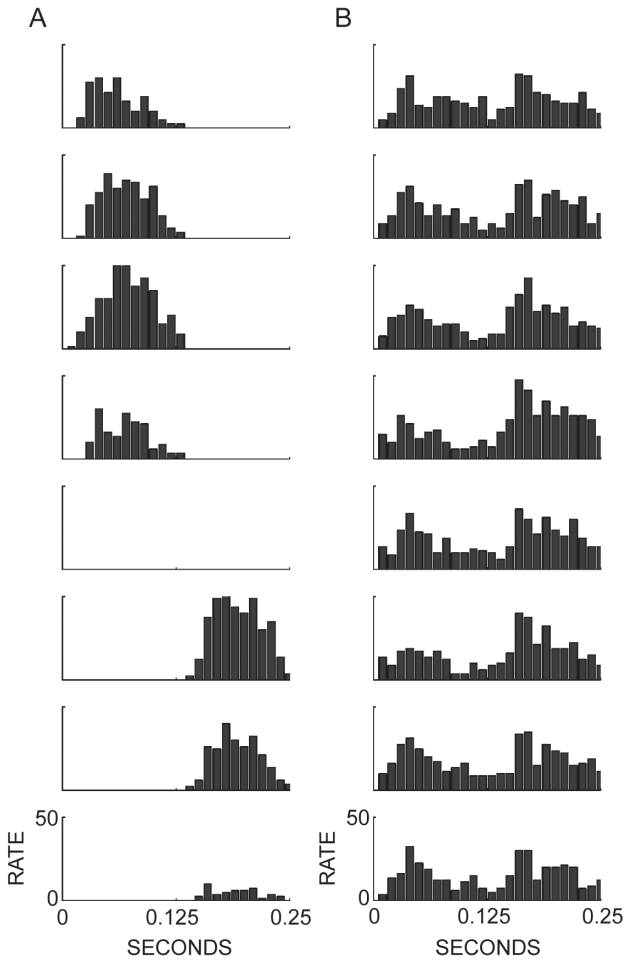

Fig. 2. Responses of model neurons to contrast reversal (8 spatial phases, at optimal orientation, and temporal and spatial frequency). *A* and *B* are cycle-averaged firing rates of respectively a simple and complex neuron in the model network. *A*: Simple cell was driven at 4 Hz in model network. The spatial phase is defined so that one spatial cycle of the grating pattern is 360°. At 180°, the response is zero. *B*: Complex cell was driven at 4 Hz in model network. The response is at the second harmonic and is insensitive to spatial phase. Cycle averages are performed over 24 cycles. The figure is reproduced from Tao *et al.* [17].

performed over a large number (say, 100 neurons or more), statistically the frequency-doubled synaptic inputs are insensitive to the spatial phase of the contrast-reversing grating. Furthermore, because of frequency-doubled synaptic inputs, both intracortical excitatory and intracortical inhibitory conductances are also frequency doubled in time. Therefore, when the excitation is sufficiently strong to drive the neuron to fire, the neuron will fire in a frequency-doubled fashion and appear as a complex cell.

Trade-off between LGN and cortico-cortical input: Phase insensitivity and frequency doubling are key to how this network produces both simple and complex cells. For example, Fig. 2*B* shows that LGN excitation is frequency doubled at the orthogonal phase, yet this strong nonlinearity in the LGN input is not expressed in the spiking of the cell. As explained in Wielaard *et al*. [22], if excitation and cortico-cortical inhibition are roughly in balance, phase insensitive cortico-cortical inhibition is sufficient to suppress frequency-doubled firing at the orthogonal phase.

An important structural element of our model is that the number of excitatory, LGN afferents driving a cortical cell is inversely correlated to the number of excitatory cortico-cortical afferents. That is, the fewer synapses on a cell taken up by the LGN, the more are available to excitatory (presynaptic) neurons in the network. The consequences of this assumption can be seen in Fig. 4. Thus naturally this network can produce cells with highly phase-specific responses (simple) and cells with phase-insensitive responses (complex) and cells with an intermediate level of spatial phase specificity.

2.2 Drifting grating responses and the modulation ratio

Another common visual stimulus used to classify the response properties of cortical neurons is drifting gratings (a traveling, spatially modulated intensity pattern, held at a fixed orientation). Often used to probe selectivities for orientation, frequency, or direction, this stimulus also evokes characteristic differences between simple and complex cells. For the model simple and complex cells represented in Fig. 2 and 4, Fig. 4 displays their extra- and intra-cellular responses to a drifting grating stimulus (8 Hz at optimal orientation and spatial frequency). Their extracellular responses are typical of experimentally observed simple and complex cells: The simple cell follows the temporal modulation of the grating as the grating drifts across its receptive field, whereas the complex cell shows an elevated, mostly constant firing over the entire duration of the stimulation.

Examination of LGN and cortico-cortical conductances in Fig. 5 accounts for the model's response to drifting gratings. First, the strong LGN excitation into the simple cell modulates with the stimulus frequency. Different cells receive LGN excitation of similar wave-

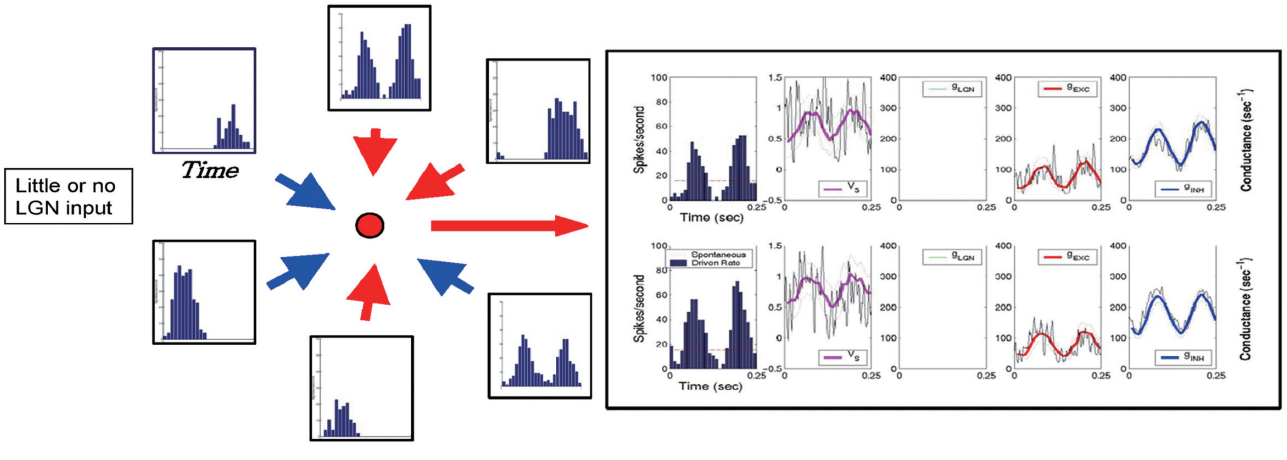

Fig. 3. Left, a schematic of synaptic inputs (pictured as neuronal firing rates in time of 6 sample neurons, over one single cycle of a contrast-reversing sinusoidally modulated grating at a particular spatial phase) that might be pooled to drive a sample complex cell in the network. Right, a model complex cell at two different spatial phases. From left to right: cycle-averaged firing rate (with the spontaneous rate in red dashes); effective reversal potential V_S; LGN conductance (green); cortico-cortical excitatory conductance (red); cortico-cortical inhibitory conductance (blue). Thin black lines indicate instantaneous values of conductances and potentials. Cycle averages are performed over 24 cycles.

form, but due to variability in both the number of LGN afferents, and in spatial phase preference, they are diverse in both amplitude and time of peak excitation. For drifting grating stimulation, this yields a bulk forcing to the model that is nearly constant in time and which is manifested as nearly time-invariant cortico-cortical conductances [22]. Thus, for the model simple cell, both the intracellular effective reversal potential, V_S, and its extracellular firing pattern modulate on the time dependence of its LGN input. Conversely, for the model complex cell both V_S and the firing pattern are driven by the steady cortico-cortical conductances, and hence show only elevated, unmodulated responses.

2.3 Population distributions of modulation ratio

The two cells in Fig. 5 are examples taken from a continuum of possible intracellular and extracellular responses. We explore this with a standard characterization of response: Figure 6*A* shows the histogram of the modulation ratio F1/F0 of the cycle-averaged effective reversal potential, V_S, across the whole population of approximately 3 000 excitatory neurons within the model. The modulation ratio is the ratio of the amplitude of the first harmonic (at the stimulus frequency) to the mean. Cells with nearly constant in time intracellu-

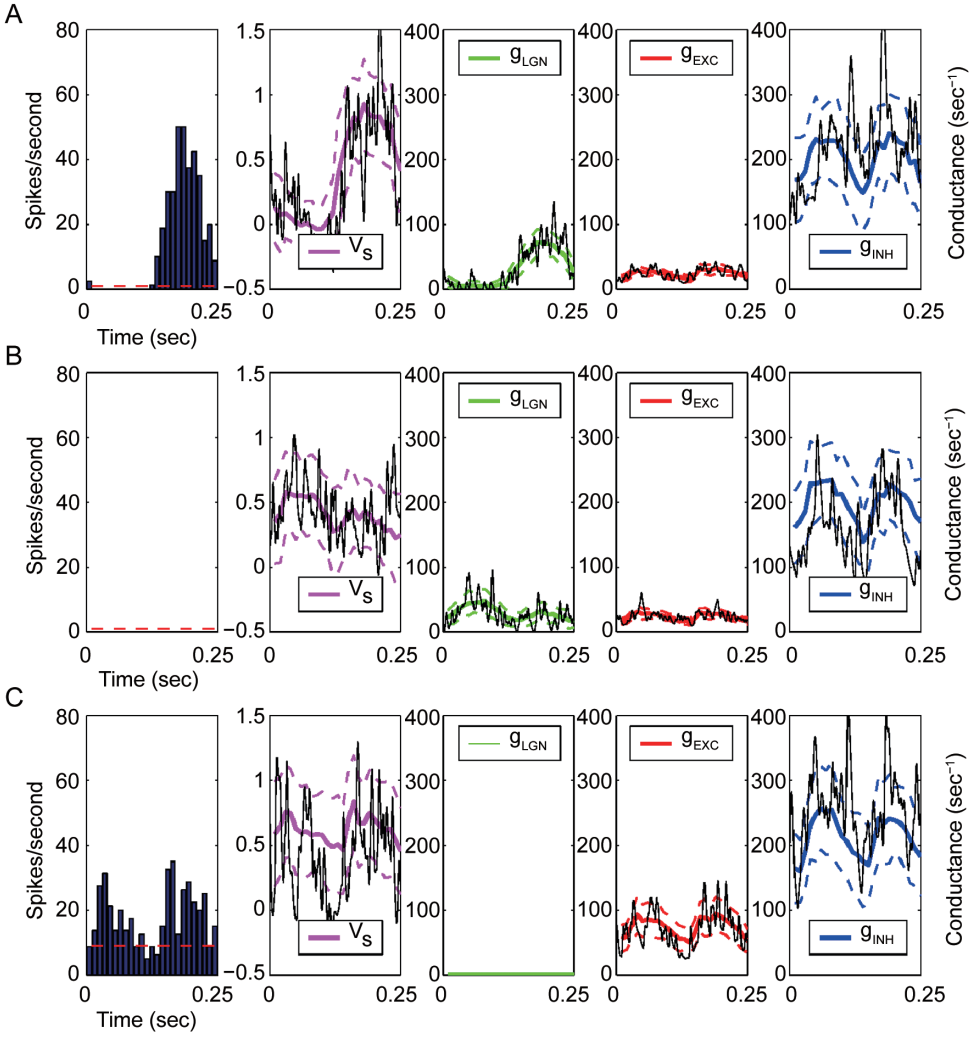

Fig. 4. Extra- and intracellular responses to 4 Hz contrast reversal. *A* and *B* show the model simple cell in Fig. 2*A* responding at its preferred and orthogonal spatial phases. *C*: Model complex cell in Fig. 2*B* at one of the phases. From left to right: cycle-averaged firing rate (with the spontaneous rate in red dashes); effective reversal potential V_S; LGN conductance (green); cortico-cortical excitatory conductance (red); cortico-cortical inhibitory conductance (blue). Dotted lines are standard deviations for each of the conductances and for the potential. Thin black lines indicate instantaneous values of conductances and potentials. Cycle averages are performed over 24 cycles. The figure is reproduced from Tao *et al.* [17].

lar responses, like the sample complex cell in Fig. 5*B*, have modulation ratios near zero. Cells temporally modulating with the stimulus, like the simple cell in Fig. 5*A*, have modulation ratios near two.

The population distribution of modulation ratio is broad, unimodal and monotonically decreasing, and re-

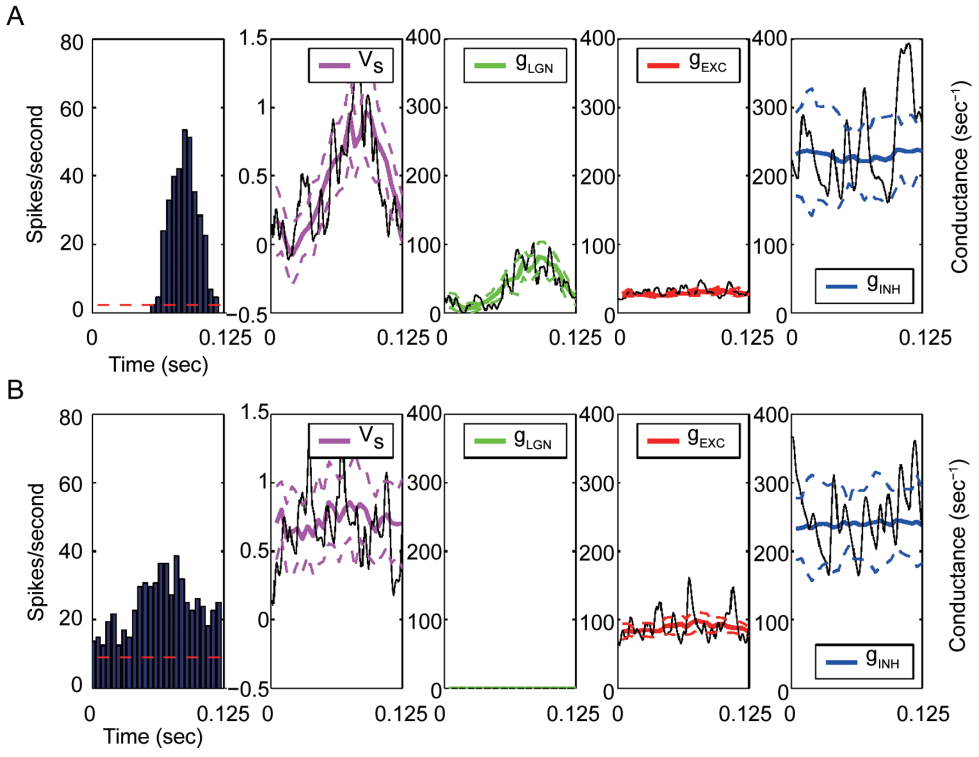

Fig. 5. Cellular responses to 8 Hz drifting grating at optimal orientation: *A*: The model simple cell in Fig. 2*A*; *B*: The model complex cell in Fig. 2*B*. From left to right: cycle-averaged firing rates (spontaneous rates as dashed red lines); effective reversal potential V_S (magenta); LGN conductance (green); cortico-cortical excitatory conductance (red); cortico-cortical inhibitory conductance (blue). The dotted lines are standard deviations for each of the conductances and for the potential. The thin black lines indicate instantaneous values of conductances and potentials. Cycle-averages are performed over 48 cycles. The figure is reproduced from Tao *et al.* [17].

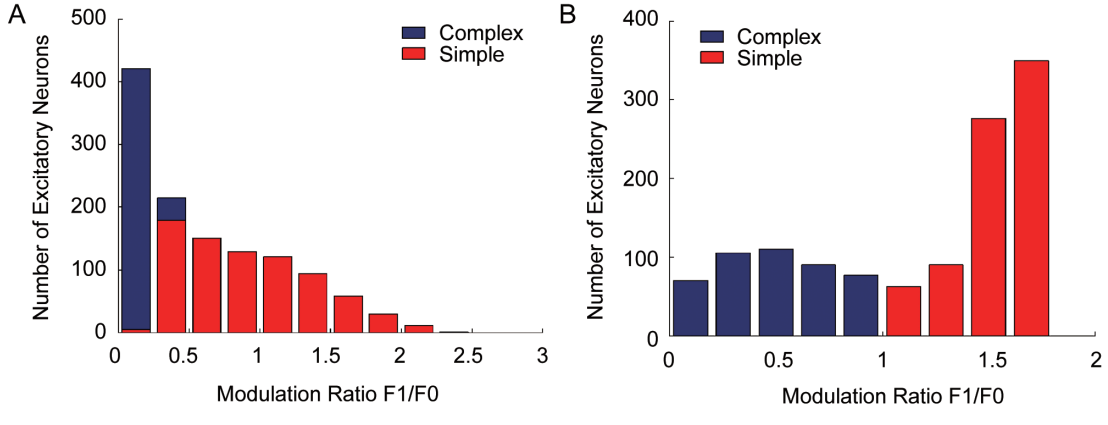

Fig. 6. Comparison of intracellular and extracellular modulation ratio F1/F0 between model and experiment. *A*: Distribution of F1/F0 of membrane potential (relative to background activity) of excitatory neurons in our model network. The height of each bar indicates the total number of excitatory neurons in each bin, while the blue and red portions correspond to the cells that are classified as "simple" or "complex" based on their extracellular responses. *B*: Distribution of the modulation ratio F1/F0 of the firing rate for excitatory neurons in model network (The distribution for the inhibitory population is qualitatively similar). For these two distributions, only cells with mean rates above 8 spikes/s are included. The figure is reproduced from Tao *et al.* [17].

flects the broad distribution in number of LGN afferents and the constraint of fixed total excitation. In unpublished work, David Ferster and colleagues measured the modulation ratio of the intracellular potential for 168 cells in cat cortex (personal communication; see Fig. 11 of Carandini *et al*. [39] for an analysis on a much smaller set of cat V1 cells). Like our model here, their measurements show also a broad and unimodal distribution of intracellular F1/F0.

However, this unimodality is not preserved in extracellular measures. Fig. 6*B* shows for the model cortex the distribution of modulation ratio of the cycle-averaged firing rate. Following others (e.g. Ringach *et al*. and Skottun *et al*. [5, 40]), we use this extracellular F1/F0 as a classifier, labeling those cells with F1/F0 > 1 as simple (red in Fig. 6), and those with F1/F0 < 1 as complex (blue in the Fig. 6). Qualitatively similar, both the distribution from our model and from various experiments show a bimodal structure peaked near the extremes of the classifier, but with a large proportion of cells having responses that are neither wholly simple, nor wholly complex.

Mechler and Ringach [41] have shown that spike-rate rectification could lead to a bimodal distribution in extracellular F1/F0, even though intracellular response is unimodally distributed (also see Abbott *et al*. [42]). Our work here shows that this result can arise within a network model which incorporates many elements that are biologically realistic.

3 Discussion

The main purpose of this review was to recapitulate some essential V1 modeling results scattered in the literature for the convenience of the reader. Here we have presented results of a neuronal network model, based on mammalian V1, for the emergence of simple and complex cells within a single basic neuronal circuit. In this model, the different types of physiological responses reflect the underlying distribution of geniculate versus cortico-cortical excitation. While the amount of excitation is kept roughly fixed, its division varies widely from cell to cell, as do many other elements of the model, such as strength of coupling and of extra-cortical drive, and the receptive field properties of convergent LGN excitation. Consistent with experiment measurement, many cells emerge as complex, many as simple, and many as being in between, the model predicts a bimodal but broad structure of extracellular modulation ratio, itself arising from a distribution of intra-cellular modulation ratios that is broad but monotonic. This prediction is also consistent with available data.

This model is different from the influential hierarchical model of Hubel and Wiesel [1], wherein simple cells receive strong geniculate drive and their pooled output drives the complex cells. Clearly, a strict rendering of the Hubel and Wiesel model would yield a bimodal population response in both the extra- and intra-cellular modulation ratio, as is not observed here, nor in the experiments. Our model is more egalitarian than hierarchical, with all cell types receiving strong inputs from the network and with almost all cells receiving LGN drive.

A crucial feature of our model is cortico-cortical inhibition, which allows the possibility of nearly linear, simple cell responses in the network, even when driven by LGN cells with their attendant rectification nonlinearities [22].

While our model is motivated by an interpretation of macaque V1 cortical architecture [22, 23] and realized in a large-scale computational model with spiking neurons, it shares important features with the modeling of Chance *et al*. [43], where the cortico-cortical, recurrent excitation plays a central role in creating complex cell responses. However, in our model recurrent excitation does not so much play the role of yielding phase invariant responses, as in Chance *et al*.[43], but rather in yielding sufficiently high, physiologically reasonable firing rates for complex cells that are also being inhibited. Phase invariance is built into the complex cell's total synaptic input by summing over both complex and simple cells indiscriminately and nonspecifically. In an elaboration of their basic model, Chance *et al*.[43] also demonstrated that a mixed population of simple, complex, and intermediate cells could be found by randomly varying the strength of connectivity to the model cortical network.

Finally, we have emphasized in this review the form of the model's cycle- or time-averaged responses. However, the examinations of Fig. 4 and 5 show that instantaneous values of V_S and the conductances are strongly fluctuating, with the mean V_S mostly below, or barely above, the threshold to firing. Clearly, fluctuations are important to creating the network state. Furthermore, as large ranges in coupling parameters were explored, regions where multistable and hysteretic behavior (with respect to stimulus parameters) were un-

covered, we found that stable and physiologically realistic behavior can only be maintained by adding background noise. It is at this point when we realized the importance of fluctuations in the membrane potential and synaptic conductances, issues which we do not have space to address in this review but instead refer the readers to Tao *et al*. [24].

REFERENCES

1 Hubel DH, Wiesel TN. Receptive fields, binocular interaction and functional architecture in the cat's visual cortex. J Physiol 1962; 160: 106–154.

2 Movshon JA, Thompson ID, Tolhurst DJ. Spatial summation in the receptive fields of simple cells in the cat's striate cortex. J Physiol 1978; 283: 53–77.

3 Movshon JA, Thompson ID, Tolhurst DJ. Spatial and temporal contrast sensitivity of neurones in areas 17 and 18 of the cat's visual cortex. J Physiol 1978; 283: 101–120.

4 Toyama K, Kimura M, Tanaka K. Cross-correlation analysis of interneuronal connectivity in cat visual cortex. J Neurophysiol 1981; 46(2): 191–201.

5 Ringach DL, Shapley RM, Hawken MJ. Orientation selectivity in macaque V1: diversity and laminar dependence. J Neurosci 2002; 22(13): 5639–5651.

6 Hoffman KP, Stone J. Conduction velocity of afferents to cat visual cortex: a correlation with cortical receptive field properties. Brain Res 1971; 32(2): 460–466.

7 Singer W, Tretter F, Cynader M. Organization of cat striate cortex: a correlation of receptive-field properties with afferent and efferent connections. J Neurophysiol 1975; 38(5): 1080–1098.

8 Ferster D, Lindstrom S. An intracellular analysis of geniculo-cortical connectivity in area 17 of the cat. J Physiol 1983; 342: 181–215.

9 Movshon JA. The velocity tuning of single units in cat striate cortex. J Physiol 1975; 249(3): 445–468.

10 Hammond P, MacKay DM. Differential responsiveness of simple and complex cells in cat striate cortex to visual texture. Exp Brain Res 1977; 30(2–3): 275–296.

11 Malpeli JG. Activity of cells in area 17 of the cat in absence of input from layer a of lateral geniculate nucleus. J Neurophysiol 1983; 49(3): 595–610.

12 Malpeli JG, Lee C, Schwark HD, Weyand TG. Cat area 17. I. Pattern of thalamic control of cortical layers. J Neurophysiol 1986; 56(4): 1062–1073.

13 Mignard M, Malpeli JG. Paths of information flow through visual cortex. Science 1991; 251(4998): 1249–1251.

14 Ringach DL. Spatial structure and symmetry of simple-cell receptive fields in macaque primary visual cortex. J Neurophysiol 2002; 88(1): 455–463.

15 Alonso JM, Usrey WM, Reid RC. Rules of connectivity between geniculate cells and simple cells in cat primary visual cortex. J Neurosci 2001; 21(11): 4002–4015.

16 Tanaka K. Organization of geniculate inputs to visual cortical cells in the cat. Vision Res 1985; 25(3): 357–364.

17 Tao L, Shelley M, McLaughlin D, Shapley R. An egalitarian network model for the emergence of simple and complex cells in visual cortex. Proc Natl Acad Sci U S A 2004; 101(1): 366–371.

18 Miller KD. Synaptic economics: competition and cooperation in synaptic plasticity. Neuron 1996; 17(3): 371–374.

19 Miller KD, MacKay D. The role of constraints in Hebbian learning. Neural Comput 1994; 6: 100–126.

20 Royer S, Pare D. Bidirectional synaptic plasticity in intercalated amygdala neurons and the extinction of conditioned fear responses. Neuroscience 2002; 115(2): 455–462.

21 Royer S, Pare D. Conservation of total synaptic weight through balanced synaptic depression and potentiation. Nature 2003; 422(6931): 518–522.

22 Wielaard DJ, Shelley M, McLaughlin D, Shapley R. How simple cells are made in a nonlinear network model of the visual cortex. J Neurosci 2001; 21(14): 5203–5211.

23 McLaughlin D, Shapley R, Shelley M, Wielaard DJ. A neuronal network model of macaque primary visual cortex (V1): orientation selectivity and dynamics in the input layer 4Calpha. Proc Natl Acad Sci U S A 2000; 97(14): 8087–8092.

24 Tao L, Cai D, McLaughlin DW, Shelley MJ, Shapley R. Orientation selectivity in visual cortex by fluctuation-controlled criticality. Proc Natl Acad Sci U S A 2006; 103(34): 12911–12916.

25 Lapicque L. Recherches quantitatives sur l'excitation electrique des nerfs traitee comme une polarization. J Physiol Pathol Gen 1907; 9: 620–635.

26 Kuffler SW. Discharge patterns and functional organization of mammalian retina. J Neurophysiol 1953; 16(1): 37–68.

27 Hubel DH, Wiesel TN. Receptive fields of optic nerve fibres in the spider monkey. J Physiol 1960; 154: 572–580.

28 Wiesel TN, Hubel DH. Spatial and chromatic interactions in the lateral geniculate body of the rhesus monkey. J Neurophysiol 1966; 29(6): 1115–1156.

29 Gielen CC, van Gisbergen JA, Vendrik AJ. Characterization of spatial and temporal properties of monkey LGN Y-cells. Biol Cybern 1981; 40: 157–170.

30 Benardete EA, Kaplan E. Dynamics of primate P retinal ganglion cells: responses to chromatic and achromatic stimuli. J Physiol 1999; 519 Pt 3: 775–790.

31 Benardete EA, Kaplan E. The dynamics of primate M retinal ganglion cells. Vis Neurosci 1999; 16(2): 355–368.

32 Somers DC, Nelson SB, Sur M. An emergent model of orientation selectivity in cat visual cortical simple cells. J Neu-

rosci 1995; 15(8): 5448–5465.
33 Troyer TW, Krukowski AE, Priebe NJ, Miller KD. Contrast-invariant orientation tuning in cat visual cortex: thalamocortical input tuning and correlation-based intracortical connectivity. J Neurosci 1998; 18(15): 5908–5927.
34 Reid RC, Alonso JM. Specificity of monosynaptic connections from thalamus to visual cortex. Nature 1995; 378(6554): 281–284.
35 DeAngelis GC, Ghose GM, Ohzawa I, Freeman RD. Functional micro-organization of primary visual cortex: receptive field analysis of nearby neurons. J Neurosci 1999; 19(10): 4046–4064.
36 Mechler F, Reich DS, Victor JD. Detection and discrimination of relative spatial phase by V1 neurons. J Neurosci 2002; 22(14): 6129–6157.
37 De Valois RL, Albrecht DG, Thorell LG. Spatial frequency selectivity of cells in macaque visual cortex. Vision Res 1982; 22(5): 545–559.
38 Spitzer H, Hochstein S. Simple- and complex-cell response dependences on stimulation parameters. J Neurophysiol 1985; 53(5): 1244–1265.
39 Carandini M, Ferster D. Membrane potential and firing rate in cat primary visual cortex. J Neurosci 2000; 20(1): 470–484.
40 Skottun BC, De Valois RL, Grosof DH, Movshon JA, Albrecht DG, Bonds AB. Classifying simple and complex cells on the basis of response modulation. Vision Res 1991; 31(7–8): 1079–1086.
41 Mechler F, Ringach DL. On the classification of simple and complex cells. Vision Res 2002; 42(8): 1017–1033.
42 Abbott LF, Chance FS. Rethinking the taxonomy of visual neurons. Nat Neurosci 2002; 5(5): 391–392.
43 Chance FS, Nelson SB, Abbott LF. Complex cells as cortically amplified simple cells. Nat Neurosci 1999; 2(3): 277–282.

* * * * *

About the author: TAO Louis

TAO Louis received his A.B. in Physics at Harvard University in 1990 and his Ph. D. in Physics at the University of Chicago in 1995. After postdoctoral positions in Cambridge (UK), Columbia University and New York University, he was an assistant professor in the Department of Mathematical Sciences at New Jersey Institute of Technology from 2003–2007. He is currently a Principal Investigator at the College of Life Sciences at Peking University. His current research interests are in mathematical neuroscience and computational biology.